The 2009 IEEE/RSJ International Conference on
Intelligent Robots and Systems
October 11-15, 2009 St. Louis, USA

Implementation of a Foldable 3 DOF Master Device to Handle a Large Glass Plate

Jaeheon Chung, Jong Tae Seo, Byung-Ju Yi, Whee Kuk Kim, and Sang Heon Lee

Abstract— **This paper proposes a new spatial 3-DOF parallel mechanism with a unique forward kinematic solution. Using the Scott mechanism as its sub-chain, the mechanism is foldable, which is useful for design of a compact-sized master device. The kinematics of this mechanism is derived and its kinematic characteristics are analyzed in terms of workspace and kinematic isotropy. The mechanism was implemented and tested as a master device to control a virtual construction robot handling a large glass plate.**

I. Introduction

PARALLEL mechanisms have been extensively studied. Less degree-of-freedom (DOF) parallel mechanisms have drawn much attention these days since they are cheap, easy to develop, and have more applications as compared to 6-DOF parallel mechanism. The 3-DOF parallel mechanism is classified into 3T (translation) type, 3R (rotation) type, 2T-1R type, and 1T-2R type. This paper focuses on application of the 1T-2R type.

Hertz and Hughes [1] analyzed a general double-tripod parallel manipulator with 3-RSR. Ceccarelli [2] proposed a spatial parallel mechanism that was composed of leg mechanisms containing articulated parallelograms and a peculiar connection with ball joints and prismatic guides. Carretero, et al. [3, 4] proposed a mechanism with 3-PRS structure. Merlet [5] proposed a spatial parallel mechanism with 3-PRS, applied to an endoscope. Lee and Shah [6] addressed a parallel mechanism with 3-RPS structure. Chung, et al. [7] proposed a parallel structure with 3-PRS structure using hinge mechanisms. Chung, et al. [8] proposed a parallel mechanism, which is composed of 2-RPS and 1-PSP chains, as a flat panel TV mounting device.

This work was partially supported by the Korea Science and Engineering Foundation (KOSEF) grant funded by the Korea government (R01-2008-000-11742-0), partially supported by the GRRC program of Gyeonggi province (2008-041-0003 -0001), partially supported by the research fund of HYU (HYU-2008-T), partially supported by the Ministry of Knowledge Economy (MKE) and Korea Industrial Technology Foundation (KOTEF) through the Human Resource Training Project for Strategic Technology, and the outcome of a Manpower Development Program for Energy & Resources supported by the Ministry of Knowledge and Economy (MKE).

J. Chung and J. T. Seo are with School of Electrical Engineering and Computer Science, Hanyang University, Ansan, Korea. (e-mail: jaeheon.chung@gmail.com and jt1000je@naver.com).

B.-J. Yi is with School of Electrical Engineering and Computer Science, Hanyang University, Ansan, Korea. (corresponding author phone: +82-31-400-5218; fax: +82-31-416-6416; e-mail: bj@ hanyang.ac.kr).

W. K. Kim is with Department of Control and Instrumentation Engineering, Korea University, Korea. (e-mail:wheekuk@korea.ac.kr).

S. H. Lee is with Institute of Construction Technology, Samsung C&T Corporation, Korea. (e-mail:shlee31@samsung.com)

Though many 1T-2R type parallel mechanisms have been designed, they are not adequate to master devices because of not having unique forward kinematic solution. Thus, this paper proposes a new 1T-2R type 3-DOF parallel mechanism with a unique forward kinematic solution. Using the Scott mechanism as its sub-chain, the mechanism is foldable, which is useful for design of a compact-sized master device.

Various types of robots have been researched in the field of construction area since the early 1980's. It is to cope with several problems such as lack of skillful labors, productivity, and quality in construction sites. Lots of construction equipments are being used in the sites and they lessen the laboriousness and improve productivity in these days. But researches on robotization in construction are still demanding to meet the increase of heavy construction materials. A glass plate is a typical one of the most heavy and fragile finishing materials. Moreover fitting a glass is a subtle process that requires a tight accuracy. So automation of installing a glass is a remarkably challenging subject.

In this paper, we focus on the design of a master robot which is used for fitting a large glass plate into the window of high-rise buildings. The construction system has a form of a hydraulic lifter equipped with the robotic mechanism at the manipulator's tip. The robotic mechanism is the slave system capable of fine motion. A parallel mechanism is utilized as a force-reflecting master device to control the fine motion in the last stage of the glass fitting task.

The structure of this device is explained in section II. Section III deals with the kinematic modeling. Experiment of the mechanism is performed in section IV. Finally, section V draws the conclusion.

II. Structure

A proposed mechanism consists of a base plate, a top plate, and three sub-chains connecting the two plates together. Each sub-chain employs Scott mechanism [9] which consists of three revolute joints and one prismatic joint. The three Scott mechanisms are arranged parallel to each other for the base plate to have a small area. Thus, it can be used as a compact-sized foldable master device. The desired operation of this mechanism can be described as follows. The end of the Scott mechanism moves along the line of $\overline{P_iB_i}$ as shown in Fig. 1. Full extension or compression of the three chains creates a pop-out or a pop-in motion of the top plate. Movement of the left chain and right chain in an opposite direction while fixing the position of the center chain located at the center position creates a swivel motion. Extension of the left-chain and right-chain with compression of the center chain or vice versa creates a tilting motion.

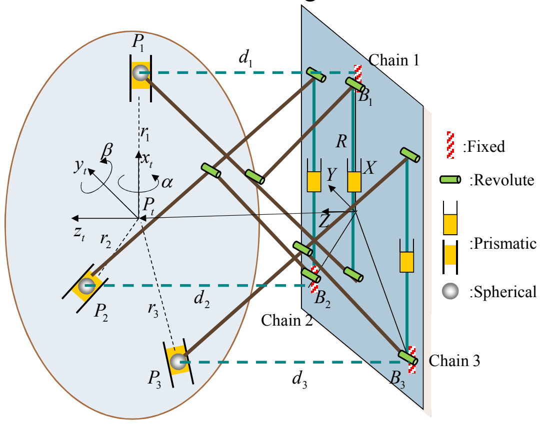

Fig. 1. Kinematic model

III. KINEMATICS

A. Description of Coordinates

The proposed mechanism has 3-DOF in space. In Fig. 1, the independent outputs are the displacement along the global Z axis and two rotational angles of the top plate about the x_t and y_t axes of the top plate's coordinate frame (i.e., the tilting angle β about the y_t -axis and the swivel angle α about the x_t -axis). The rest three outputs x_t, y_t, and γ (i.e., the roll motion about the z_t-axis) are dependent outputs.

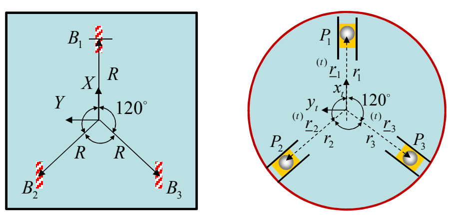

(a) (b)

Fig. 2. Coordinates, (a) Base plate, (b) Top plate

Denote $\underline{P}_t = \begin{bmatrix} x_t & y_t & z_t \end{bmatrix}^T$ as the position vector from the origin of the base frame to the origin of the top plate frame. Fig. 2 shows coordinates of the base and the top plates. $\underline{B}_i$ represents the position vector from the origin of the base plate to the fixed point of the i-th chain, and it can be expressed as

$$\underline{B}_1 = \begin{bmatrix} R & 0 & 0 \end{bmatrix}^T, \quad (1)$$

$$\underline{B}_2 = \begin{bmatrix} -\tfrac{1}{2}R & \tfrac{\sqrt{3}}{2}R & 0 \end{bmatrix}^T, \quad (2)$$

and

$$\underline{B}_3 = \begin{bmatrix} -\tfrac{1}{2}R & -\tfrac{\sqrt{3}}{2}R & 0 \end{bmatrix}^T. \quad (3)$$

$\underline{P}_i$ denotes the position vector from the origin of the base plate to the i-th spherical joint (P_i), and it can be expressed as

$$\underline{P}_1 = \begin{bmatrix} R & 0 & d_1 \end{bmatrix}, \quad (4)$$

$$\underline{P}_2 = \begin{bmatrix} -\tfrac{1}{2}R & \tfrac{\sqrt{3}}{2}R & d_2 \end{bmatrix}^T, \quad (5)$$

and

$$\underline{P}_3 = \begin{bmatrix} -\tfrac{1}{2}R & -\tfrac{\sqrt{3}}{2}R & d_3 \end{bmatrix}^T, \quad (6)$$

where d_i denotes the distance from $\underline{B}_i$ to $\underline{P}_i$.

In Fig. 3, the position B_i is fixed to the base plate and the position A_i is displaced along the TM screw. The movement of the point P_i along the line P_iB_i is equivalent to the displacement d_i of the prismatic joint. Extension of the Scott mechanism can be controlled by the displacement of the prismatic joint d_{bi} in the Scott mechanism. Importantly, designing the length of the three links identical makes this Scott mechanism foldable. The relationship between d_{bi} and d_i can be expressed as

$$d_i = \sqrt{4l^2 - d_{bi}^2}. \quad (7)$$

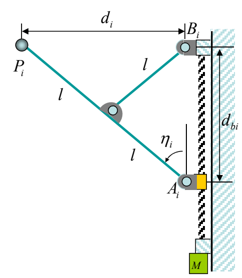

Fig. 3. Kinematic model of the Scott mechanism

The position vector ${}^{(t)}\underline{r}_i$ with respect to the local coordinate system fixed on the top plate is described as

$${}^{(t)}\underline{r}_1 = \begin{bmatrix} r_1 & 0 & 0 \end{bmatrix}^T, \quad (8)$$

$${}^{(t)}\underline{r}_2 = \begin{bmatrix} -\tfrac{1}{2}r_2 & \tfrac{\sqrt{3}}{2}r_2 & 0 \end{bmatrix}^T, \quad (9)$$

and

$${}^{(t)}\underline{r}_3 = \begin{bmatrix} -\tfrac{1}{2}r_3 & -\tfrac{\sqrt{3}}{2}r_3 & 0 \end{bmatrix}^T. \quad (10)$$

Using the $x-y-z$ Euler angle set, the rotation matrix $\begin{bmatrix} R_t^b \end{bmatrix}$ of the output frame is denoted as

$$[R_t^b] = [Rot(x,\alpha)][Rot(y,\beta)][Rot(z,\gamma)]$$
$$= \begin{bmatrix} c_\beta c_\gamma & -c_\beta s_\gamma & s_\beta \\ s_\alpha s_\beta c_\gamma + c_\alpha s_\gamma & -s_\alpha s_\beta s_\gamma + c_\alpha c_\gamma & -s_\alpha c_\beta \\ -c_\alpha s_\beta c_\gamma + s_\alpha s_\gamma & c_\alpha s_\beta s_\gamma + s_\alpha c_\gamma & c_\alpha c_\beta \end{bmatrix}, \quad (11)$$

where $Rot(x,\alpha)$ denotes the rotation about the x-axis by α angle. c_α and s_α denote the $\cos(\alpha)$ and $\sin(\alpha)$, respectively. Simply, (11) can be expressed as

$$[R_t^b] = \begin{bmatrix} \underline{\hat{x}}_t & \underline{\hat{y}}_t & \underline{\hat{z}}_t \end{bmatrix} = \begin{bmatrix} r_{11} & r_{12} & r_{13} \\ r_{21} & r_{22} & r_{23} \\ r_{31} & r_{32} & r_{33} \end{bmatrix}. \quad (12)$$

B. Forward Kinematics

Forward kinematics is to find the output position and orientation of the mechanism when the input variables are known. The forward position analysis of this mechanism consists of three stages. Firstly, displacements of prismatic joints (r_1 , r_2 , and r_3) at the top plate are obtained from a geometry of the top plate. Secondly, the output position is obtained from the values of r_1 , r_2 , and r_3 . Finally, the output orientation is obtained from the output position and the geometry of the top plate.

1) Output position

The variables d_i in the Scott mechanism is calculated for the given input d_{bi} . Then, the position of $\underline{P}_1$, $\underline{P}_2$, and $\underline{P}_3$ are known. First of all, the position vector $\underline{P}_i$ with respect to the base frame can be expressed as

$$\underline{P}_i = \begin{bmatrix} P_{ix} & P_{iy} & P_{iz} \end{bmatrix}^T \text{, for } i\text{=1, 2, and 3.} \tag{13}$$

Then, the vector $\underline{Z}_t$ that is perpendicular to the top plate can be expressed as

$$\underline{Z}_t = \left(\underline{P}_2 - \underline{P}_1\right)\times\left(\underline{P}_3 - \underline{P}_1\right) = \begin{bmatrix} Z_{f1} & Z_{f2} & Z_{f3} \end{bmatrix}^T, \tag{14}$$

where

$$\begin{aligned} Z_{f1} &= -P_{1z}P_{2y} + P_{1y}P_{2z} + P_{1z}P_{3y} \\ &\quad - P_{2z}P_{3y} - P_{1y}P_{3z} + P_{2y}P_{3z}, \end{aligned} \tag{15}$$

$$\begin{aligned} Z_{f2} &= P_{1z}P_{2x} - P_{1x}P_{2z} - P_{1z}P_{3x} \\ &\quad + P_{2z}P_{3x} + P_{1x}P_{3z} - P_{2x}P_{3z}, \end{aligned} \tag{16}$$

and

$$\begin{aligned} Z_{f3} &= -P_{1y}P_{2x} + P_{1x}P_{2y} + P_{1y}P_{3x} \\ &\quad - P_{2y}P_{3x} - P_{1x}P_{3y} + P_{2x}P_{3y}. \end{aligned} \tag{17}$$

From (12) and (14), the vector $\hat{\underline{z}}_t$ can be expressed as

$$\hat{\underline{z}}_t = \frac{\underline{Z}_t}{\left\|\underline{Z}_t\right\|} = \begin{bmatrix} s_\beta \\ -s_\alpha c_\beta \\ c_\alpha c_\beta \end{bmatrix} = \begin{bmatrix} r_{13} \\ r_{23} \\ r_{33} \end{bmatrix}. \tag{18}$$

In Fig. 6, the top plate contains three passive prismatic joints (r_1 , r_2 , and r_3) and three spherical joints (P_1 , P_2 , and P_3). There is a triangle that is made by connecting with P_1 , P_2 , and P_3 . $\angle P_1P_tP_2$, $\angle P_2P_tP_3$, and $\angle P_3P_tP_1$ denote Ψ_{12} , Ψ_{23} , and Ψ_{31} , respectively. r_i denotes the distance from the point P_t to the point P_i . $\angle P_tP_1P_2$ and $\angle P_tP_1P_3$ denote θ_{1r} and θ_{1l}, respectively. Using the law of sines, $\Delta P_tP_1P_2$ and $\Delta P_tP_1P_3$ can be expressed as

$$\frac{s_{\theta_{1r}}}{r_2} = \frac{s_{\Psi_{12}}}{P_{12}} = \frac{s_{\theta_{2l}}}{r_1} \tag{19}$$

and

$$\frac{s_{\theta_{1l}}}{r_3} = \frac{s_{\Psi_{31}}}{P_{13}} = \frac{s_{\theta_{3r}}}{r_1}, \tag{20}$$

where P_{12} and P_{13} denote the distance from the point P_1 to the point P_2 and from the point P_1 to the point P_3 , respectively. As shown in Fig. 6, θ_{1l} , θ_{2l} , and θ_{3r} can be expressed as

$$\theta_{1l} = \theta_1 - \theta_{1r}, \tag{21}$$

$$\theta_{2l} = \pi - \Psi_{12} - \theta_{1r}, \tag{22}$$

and

$$\begin{aligned} \theta_{3r} &= \pi - \Psi_{31} - \theta_{1l} \\ &= \pi - \Psi_{31} - \theta_1 + \theta_{1r}. \end{aligned} \tag{23}$$

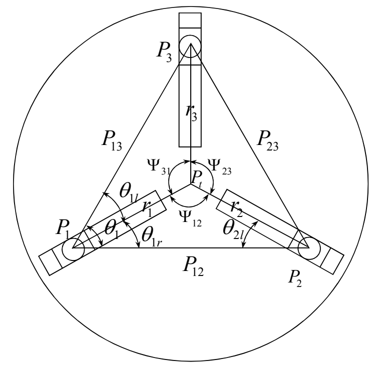

Fig. 4. Geometry of top plate

Using the law of cosines for $\Delta P_2P_1P_3$, θ_1 can be expressed as

$$\theta_1 = \cos^{-1}\frac{P_{13}^2 + P_{12}^2 - P_{23}^2}{2P_{12}P_{13}}, \tag{24}$$

where P_{23} denotes the distance from the point P_2 to the point P_3 . From (19) and (20), r_1 can be expressed as

$$r_1 = \frac{P_{12}}{\sin\Psi_{12}}\sin\left(\Psi_{12} + \theta_{1r}\right) \tag{25}$$

and

$$r_1 = \frac{P_{13}}{\sin\Psi_{31}}\sin\left(\Psi_{31} + \theta_1 - \theta_{1r}\right). \tag{26}$$

By rearranging (25) and (26) in terms of θ_{1r} , θ_{1r} can be obtained as

$$\theta_{1r} = \operatorname{atan}\left\{\frac{\dfrac{P_{13}}{\sin\Psi_{31}}\sin\left(\Psi_{31} + \theta_1\right) - P_{12}}{\dfrac{P_{13}}{\sin\Psi_{31}}\cos\left(\Psi_{31} + \theta_1\right) + \dfrac{P_{12}}{\tan\Psi_{12}}}\right\}. \tag{27}$$

From (23) and (24), r_2 and r_3 can be obtained as

$$r_2 = \frac{s_{\theta_{1r}}}{s_{\psi_{12}}}P_{12} \tag{28}$$

and

$$r_3 = \frac{s_{\theta_{1l}}}{s_{\psi_{31}}}P_{13}. \tag{29}$$

Three constraint equations are required to find x_t, y_t, and z_t from r_1 , r_2 , and r_3 . The first equation is derived as follows. At the top plate, we have

$$\underline{r}_1 = \underline{P}_1 - \underline{P}_t \tag{30}$$

and

$$\underline{r}_2 = \underline{P}_2 - \underline{P}_t, \tag{31}$$

where $\underline{r}_i$ denotes the position vector from $\underline{P}_i$ to $\underline{P}_t$. Because the vector $\underline{r}_1 \times \underline{r}_2$ is parallel to $\hat{\underline{z}}_t$ in (12), a constraint equation can be expressed as

$$\frac{\left(\underline{r}_1 \times \underline{r}_2\right)_x}{\left(\underline{r}_1 \times \underline{r}_2\right)_z} = \frac{r_{13}}{r_{33}}, \tag{32}$$

where from (30) and (31), $\underline{r}_1 \times \underline{r}_2$ can be obtained as

$$\underline{r}_1 \times \underline{r}_2 = \begin{bmatrix} \left(P_{1z} - P_{2z}\right) y_t + \left(P_{2y} - P_{1y}\right) z_t + P_{1y} P_{2z} - P_{1z} P_{2y} \\ \left(P_{2z} - P_{1z}\right) x_t + \left(P_{2y} - P_{1y}\right) z_t + P_{1z} P_{2x} - P_{1x} P_{2z} \\ \left(P_{1y} - P_{2y}\right) x_t + \left(P_{2y} - P_{1y}\right) y_t + P_{1x} P_{2y} - P_{1y} P_{2x} \end{bmatrix}. \tag{33}$$

Rearranging (33) with respect to x_t, y_t and z_t, the first constraint equation can be expressed as

$$k_1 x_t + k_2 y_t + k_3 z_t + k_4 = 0, \tag{34}$$

where

$$k_1 = \frac{r_{13}}{r_{33}}\left(P_{1y} - P_{2y}\right), \tag{35}$$

$$k_2 = \frac{r_{13}}{r_{33}}\left(P_{2y} - P_{1y}\right) - \left(P_{1z} - P_{2z}\right), \tag{36}$$

$$k_3 = -\left(P_{2y} - P_{1y}\right), \tag{37}$$

and

$$k_4 = \frac{r_{13}}{r_{33}}\left(P_{1x} P_{2y} - P_{1y} P_{2x}\right) - \left(P_{1y} P_{2z} - P_{1z} P_{2y}\right). \tag{38}$$

The rest two constraint algebraic equations can be obtained as follow:

$$-\underline{r}_1 \cdot \left(\underline{P}_2 - \underline{P}_1\right) = r_1 P_{12} c_{\theta_{1r}} \tag{39}$$

and

$$-\underline{r}_1 \cdot \left(\underline{P}_3 - \underline{P}_1\right) = r_1 P_{13} c_{\theta_{1l}}. \tag{40}$$

Substituting (30) into (39) and (40), then two other constraint equations can be expressed as

$$\left(P_{2x} - P_{1x}\right) x_t + \left(P_{2y} - P_{1y}\right) y_t + \left(P_{2z} - P_{1z}\right) z_t + w_1 = 0 \tag{41}$$

and

$$\left(P_{3x} - P_{1x}\right) x_t + \left(P_{3y} - P_{1y}\right) y_t + \left(P_{3z} - P_{1z}\right) z_t + w_2 = 0, \tag{42}$$

where

$$\begin{aligned} w_1 = & -P_{12} r_1 \cos_{\theta_{1r}} - \left(P_{2x} - P_{1x}\right) P_{1x} \\ & - \left(P_{2y} - P_{1y}\right) P_{1y} - \left(P_{2z} - P_{1z}\right) P_{1z} \end{aligned} \tag{43}$$

and

$$\begin{aligned} w_2 = & -P_{13} r_1 \cos_{\theta_{1l}} - \left(P_{3x} - P_{1x}\right) P_{1x} \\ & - \left(P_{3y} - P_{1y}\right) P_{1y} - \left(P_{3z} - P_{1z}\right) P_{1z} \end{aligned}. \tag{44}$$

From (34), (41), and (42), the output position x_t, y_t, and z_t can be obtained as

$$\begin{bmatrix} x_t \\ y_t \\ z_t \end{bmatrix} = \begin{bmatrix} P_{2x} - P_{1x} & P_{2y} - P_{1y} & P_{2z} - P_{1z} \\ P_{3x} - P_{1x} & P_{3y} - P_{1y} & P_{3z} - P_{1z} \\ k_1 & k_2 & k_3 \end{bmatrix}^{-1} \begin{bmatrix} -w_1 \\ -w_2 \\ -k_4 \end{bmatrix}. \tag{45}$$

2) Output orientation

From (18), α and β can be obtained as

$$\alpha = \operatorname{atan2}\left(-r_{32}, r_{33}\right) \tag{46}$$

and

$$\beta = \operatorname{atan2}\left(r_{13}, \sqrt{r_{23}^2 + r_{33}^2}\right), \tag{47}$$

respectively. Another orientation γ can be obtained from following constraint:

$$\underline{r}_1 = r_1 \hat{\underline{x}}_t = \underline{P}_1 - \underline{P}_t. \tag{48}$$

From (48), γ can be obtained as

$$\gamma = \operatorname{atan2}\left(\left(P_{1y} - y_t\right) c_\alpha + \left(P_{1z} - z_t\right) s_\alpha, \left(P_{1x} - x\right) / c_\beta\right). \tag{49}$$

As a conclusion, it is remarked that the output position and orientation could be uniquely obtained for the given sensor information of three input actuators.

The kinematic dimensions of this mechanism are given in Table I. To confirm the uniqueness of the forward kinematics solution, one pose of the mechanism using the unique forward kinematics solution are shown in Fig. 5. In simulation, only the encoder values of the three inputs are given. As a result, three independent outputs are calculated and plotted in Fig. 5.

Table I: Kinematic Parameters

Parameters	Dimension
R (Radius of the base plate)	0.06[m]
l (link length of Scott mechanism)	0.05[m]

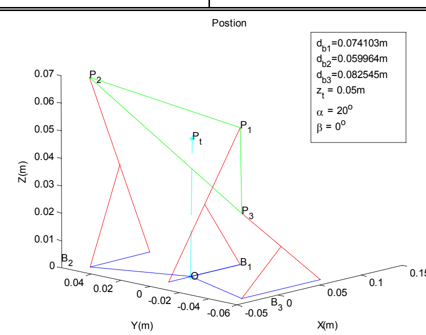

Fig. 5. Three poses of the mechanism using the unique forward kinematics

A. Inverse Kinematics

Inverse kinematics is to find the active input vector when the independent output position/orientation vector of the mechanism is given. Here, the given independent outputs are z_t, α, and β, and the three dependent outputs are x_t, y_t and γ. The position $\underline{P}_i$ with respect to the *XYZ* base frame can be expressed as

$$\underline{P}_i = \underline{P}_t + \left[R_t^b\right] {}^{(t)}\underline{r}_i, \text{ for } i\text{=1, 2 and 3} \tag{50}$$

From (50), two loop constraint equations at the top plate can be obtained as

$$\left[R_t^b\right]\left({}^{(t)}\underline{r}_1 - {}^{(t)}\underline{r}_3\right) = \underline{P}_1 - \underline{P}_3 \tag{51}$$

and

$$\left[R_t^b\right]\left({}^{(t)}\underline{r}_2 - {}^{(t)}\underline{r}_3\right) = \underline{P}_2 - \underline{P}_3. \tag{52}$$

Using (4) through (10) and (12), the above two equations can be expressed as

$$r_{11}\left(r_1+\tfrac{1}{2}r_3\right)+r_{12}\left(\tfrac{\sqrt{3}}{2}r_3\right)=\tfrac{3}{2}R\,, \tag{53}$$

$$r_{21}\left(r_1+\tfrac{1}{2}r_3\right)+r_{22}\left(\tfrac{\sqrt{3}}{2}r_3\right)=\tfrac{\sqrt{3}}{2}R\,, \tag{54}$$

$$r_{31}\left(r_1+\tfrac{1}{2}r_3\right)+r_{32}\left(\tfrac{\sqrt{3}}{2}r_3\right)=d_1-d_3\,, \tag{55}$$

$$r_{11}\left(-\tfrac{1}{2}r_2+\tfrac{1}{2}r_3\right)+r_{12}\left(\tfrac{\sqrt{3}}{2}r_2+\tfrac{\sqrt{3}}{2}r_3\right)=0\,, \tag{56}$$

$$r_{21}\left(-\tfrac{1}{2}r_2+\tfrac{1}{2}r_3\right)+r_{22}\left(\tfrac{\sqrt{3}}{2}r_2+\tfrac{\sqrt{3}}{2}r_3\right)=\sqrt{3}R\,, \tag{57}$$

and

$$r_{31}\left(-\tfrac{1}{2}r_2+\tfrac{1}{2}r_3\right)+r_{32}\left(\tfrac{\sqrt{3}}{2}r_2+\tfrac{\sqrt{3}}{2}r_3\right)=d_2-d_3\,. \tag{58}$$

From (50), the relationship between the input ($\underline{P}_i$) and the output ($\underline{P}_t$) can be obtained as

$$\underline{P}_t=\begin{bmatrix} x_t \\ y_t \\ z_t \end{bmatrix}=\underline{P}_i-\left[R_t^b\right]{}^{(t)}\underline{r}_i\,,\ \text{for } i\text{=1, 2 and 3} \tag{59}$$

The closed form inverse kinematic does not exist due to the nonlinear nature of the algebraic equations (53) through (58). The inverse kinematic solution is employed in the off-line kinematic analysis of the proposed mechanism. Thus, we employ the Newton-Raphson method to solve for the inverse kinematic solution. By using (53) through (58), the solutions of γ , r_1 , r_2 , and r_3 can be obtained by the Newon-Rhapson method. From (59), x_t , y_t , d_1 , d_2 and d_3 can be obtained as follow:

$$x_t=R-r_{11}r_1\,, \tag{60}$$

$$y_t=-r_{21}r_1\,, \tag{61}$$

$$d_1=z_t+r_{31}r_1\,, \tag{62}$$

$$d_2=z_t+\left(-\tfrac{1}{2}r_{31}+\tfrac{\sqrt{3}}{2}r_{32}\right)r_2\,, \tag{63}$$

and

$$d_3=z_t+\left(-\tfrac{1}{2}r_{31}-\tfrac{\sqrt{3}}{2}r_{32}\right)r_3\,. \tag{64}$$

Finally, the active displacement (d_{bi}) of the Scott mechanism of Fig. 3 is obtained as

$$d_{bi}=\sqrt{4l^2-d_i^2}\,. \tag{65}$$

To confirm an effectiveness of the inverse kinematics, the first video clip attached to this paper shows the real time control performance of this device.

B. First-order Kinematics

The output velocity vector of the mechanism is defined as

$$\underline{\dot{u}}=\left[\underline{\dot{P}}_t \quad \underline{\dot{\mu}}\right]^T, \tag{66}$$

where

$$\underline{\dot{P}}_t=\left[\dot{x} \quad \dot{y} \quad \dot{z}\right]^T, \tag{67}$$

and

$$\underline{\dot{\mu}}=\left[\dot{\alpha} \quad \dot{\beta} \quad \dot{\gamma}\right]^T, \tag{68}$$

$\underline{\dot{P}}_t$ and $\underline{\dot{\mu}}$ denote a linear velocity vector and an Euler velocity vector of the top plate in the operational space, respectively. Differentiating (53) through (58) with respect to time, the velocity relationship between r_1 , r_2 , r_3 , α , β , γ and the independent inputs (d_1 , d_2 , and d_3) can be obtained as

$$\begin{bmatrix} \underline{\dot{\mu}} \\ \underline{\dot{r}} \end{bmatrix}=\begin{bmatrix} \left[G_d^{\mu}\right] \\ \left[G_d^{r}\right] \end{bmatrix}\underline{\dot{d}}\,, \tag{69}$$

where the velocity vector ($\underline{\dot{r}}$) of the prismatic joint at the top plate and the independent input velocity vector($\underline{\dot{d}}$) are defined, respectively, as

$$\underline{\dot{r}}=\left[\dot{r}_1 \quad \dot{r}_2 \quad \dot{r}_3\right]^T \tag{70}$$

and

$$\underline{\dot{d}}=\left[\dot{d}_1 \quad \dot{d}_2 \quad \dot{d}_3\right]^T. \tag{71}$$

The position vector $\underline{P}_1$ of the chain 1 can be expressed as

$$\underline{P}_1=\underline{P}_t+r_1\left[R_t^b\right]\underline{\hat{x}}_t\,. \tag{72}$$

Differentiating (72) with respect to time, the output linear velocity $\underline{\dot{P}}_t$ can be obtained as

$$\underline{\dot{P}}_t=\underline{\dot{P}}_1-\frac{d}{dt}\left(r_1\left[R_t^b\right]\underline{\hat{x}}_t\right)=\underline{\dot{P}}_1-\frac{dr_1}{dt}\underline{x}_t-r_1\frac{d\underline{x}_t}{dt}\,, \tag{73}$$

where

$$\frac{dr_1}{dt}\underline{x}_t=\begin{bmatrix} r_{11} \\ r_{21} \\ r_{31} \end{bmatrix}\left[G_d^{r}\right]_{1;}\underline{\dot{d}}\,, \tag{74}$$

$$r_1\frac{d\underline{x}_t}{dt}=r_1\frac{\partial \underline{x}_t}{\partial \underline{\mu}^T}\left[G_d^{\mu}\right]\underline{\dot{d}}\,, \tag{75}$$

and

$$\underline{\dot{P}}_1=\begin{bmatrix} 0 & 0 & 0 \\ 0 & 0 & 0 \\ 1 & 0 & 0 \end{bmatrix}\underline{\dot{d}}\,. \tag{76}$$

Therefore, the relationship between the output linear velocity vector and the independent input velocity can be expressed as

$$\underline{\dot{P}}_t=\left[G_d^{P_t}\right]\underline{\dot{d}}\,, \tag{77}$$

where

$$\left[G_d^{P_t}\right]=\begin{bmatrix} 0 & 0 & 0 \\ 0 & 0 & 0 \\ 1 & 0 & 0 \end{bmatrix}-r_1\frac{\partial \underline{x}_t}{\partial \underline{\mu}^T}\left[G_d^{\mu}\right]-\begin{bmatrix} r_{11} \\ r_{21} \\ r_{31} \end{bmatrix}\left[G_d^{r}\right]_{1;}\,. \tag{78}$$

From (69) and (77), the relationship between the output velocity vector and the independent input velocity can be expressed as

$$\underline{\dot{u}}=\left[G_d^{u}\right]\underline{\dot{d}}=\begin{bmatrix} \left[G_d^{P_t}\right] \\ \left[G_d^{\mu}\right] \end{bmatrix}\underline{\dot{d}}\,. \tag{79}$$

Now, the kinematic relationship between the independent (i.e., $\dot{d}_i$) joint velocity and the active input velocity (i.e., $\dot{d}_{bi}$) is derived. In the Scott mechanism of Fig. 5, the kinematic relationship among the active prismatic joint d_{bi} , the revolute joint η_i , and the independent joint d_i are expressed as

$$d_{bi} = 2lc_{\eta_i} \tag{80}$$

and

$$d_i = 2ls_{\eta_i} \,. \tag{81}$$

Differentiating (80) and (81) with respect to time and combining the results in a matrix form yields

$$\underline{\dot{d}} = \left[G_{d_b}^{d} \right] \underline{\dot{d}}_b \,, \tag{82}$$

where

$$\left[G_{d_b}^{d} \right] = \begin{bmatrix} -1/\tan\eta_1 & 0 & 0 \\ 0 & -1/\tan\eta_2 & 0 \\ 0 & 0 & -1/\tan\eta_3 \end{bmatrix} \tag{83}$$

and $\underline{\dot{d}}_b = \left[\dot{d}_{b1} \quad \dot{d}_{b2} \quad \dot{d}_{b3} \right]^T$ denotes the active input velocity vector of the three four-bars. By substituting (82) into (79), the relationship between the output velocity vector and the active input velocity vector is obtained as

$$\underline{\dot{u}} = \left[G_{d_b}^{u} \right] \underline{\dot{d}}_b \,, \tag{84}$$

where $\underline{\dot{u}} \in R^6$ and

$$\left[G_{d_b}^{u} \right] = \left[G_{d}^{u} \right] \left[G_{d_b}^{d} \right] \in R^{6\times3} \,. \tag{85}$$

Finally, the relationship between the independent output velocity vector ($\underline{\dot{u}}_{ind}$) and the active input' velocity vector ($\underline{\dot{d}}_b$) is selected from (84).

$$\underline{\dot{u}}_{ind} = \left[\dot{z}_t \quad \dot{\alpha} \quad \dot{\beta} \right]^T = \left[G_{d_b}^{u_{ind}} \right] \underline{\dot{d}}_b \tag{86}$$

where $\left[G_{d_b}^{u_{ind}} \right] \in R^{3\times3}$ is obtained by selecting three rows of $\left[G_{d_b}^{u} \right]$, which correspond to the independent output components ($\dot{z}_t$, $\dot{\alpha}$, and $\dot{\beta}$).

IV. Implementation

The proposed mechanism in this paper has a unique forward kinematic solution. This is a good feature as a master device. Another special feature is foldability by using the Scott mechanism in its sub-chain. Thus, these features are useful for design of a compact-sized master device.

A. Implementation as a master device

Fig. 6 shows the prototype of the proposed mechanism implemented in this study and Fig. 6(b) and 6(c) shows a folded shape and an extended shape, respectively.

The information for the prismatic joint of the Scott mechanism is measured by an encoder of a DC motor connected to a TM (trapezoidal metric) screw. The resolution of the encoder is 400 pulses per turn and a pitch of the TM screw is 18mm. Based on these data, the resolution of the mechanism can be obtained as shown in Table II. This resolution is enough for precise control of a slave robot.

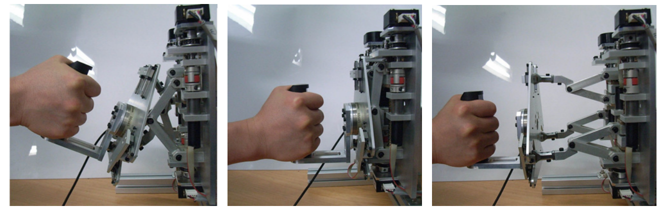

(a) (b) (c)

Fig. 6. (a) Foldable 3-DOF parallel mechanism, (b) Folded shape, (c) Extended shape

Table II: Mechanism Specification

Output	Range	Resolution
Z (Stroke)	0.08m	$11.3\mu m$
α (Swivel motion)	$\pm30^\circ$	0.0434°
β (Tilting motion)	$\pm25^\circ$	0.0251°

B. Feasibility study for application to construction robot

Glasses are widely used for the outer wall finishing of high-story buildings in these days and it can raise the aesthetic value of the building. For the task installing a large glass on the window, one of the solutions is the combination of powerful construction equipments and fine robotic mechanisms utilizing macro-micro motion control [10]. This is the best way to install large glasses on buildings because a hydraulically operated construction equipment can handle heavy materials and a delicate robot can prevent the break of brittle materials.

Yu, et al. [11] developed a curtain wall installation robot controlled by a joystick and utilized it in construction sites to evaluate its performance. We employ a master-slave system instead of the joystick and apply a force reflection algorithm to suggest an alternative improving productivity. The master-slave system helps the skillful worker to operate the system more intuitively and the force-reflection can prevent the breakage of the object.

The signal diagram of the master-slave system is shown in Fig. 7. When a user moves a handle of the master device, displacement information of the prismatic joint on the base plate is sent to the controller as the input values of the forward kinematics. The output's pose of the master device is sent to the slave controller to emulate the output's pose of the slave system.

We develop a virtual simulator to test the master device. Fig. 8 shows the virtual slave robot that handles the flat glass. The mobile robot controls the macro motion and the manipulator mounted on the mobile platform controls the small 1T-2R motion so that the panel can be fit into the window properly. Fig. 9 shows that the 1T-2R motion of the manipulator of the virtual slave robot is controlled successfully by the master device. The attached video clip demonstrates the experimental results.

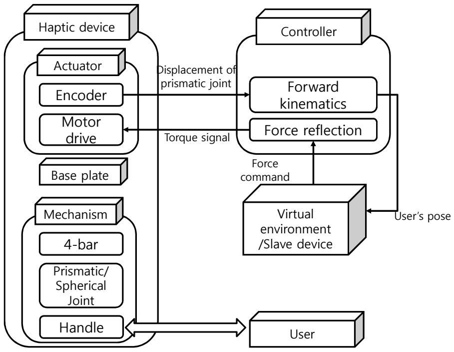

Fig. 7. Signal diagram of the master-slave system

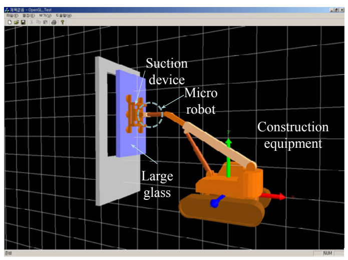

Fig. 8. Slave robot

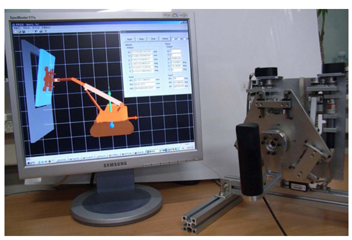

Fig. 9. Virtual simulator and master device

The performance of the force-reflection at the master device is confirmed by comparing the contact force and the measured force at the master device force. The result is shown in Fig. 10. The dotted line and the solid line represent the reflection force estimated by the simulator based on visco-elastic environment model, and the operating force that is measured by the F/T sensor attached to the handle of the master device, respectively. These results show that two forces are in proportion with each other, and it means the contact force can be effectively transferred to the operator. A negative force is measured at the master device when the master device is moving to the reverse direction as shown in Fig. 10.

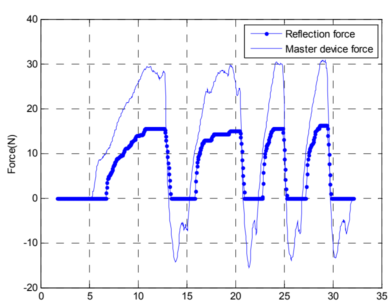

Fig. 10. Comparison between the reflection force and the measured force at the master device force

V. CONCLUSION

In this paper, a new 3-DOF parallel mechanism having 2-rotational and 1-translational motion was investigated. Contribution of this paper is the proposition of a new parallel structure that has unique forward kinematic solution and its feasibility study for application to a construction robot handling a large glass plate. As future works, we would like to implement the master device to a real construction robot system having a force feedback capability.

REFERENCES

[1] R. B. Hertz and P. C. Hughes, "Kinematic analysis of a general double-tripod parallel manipulator," *Mech. Mach. Theory*, vol. 33, no. 6, pp. 638-696, 1998.

[2] M. Ceccarelli, "A new 3 DOF spatial parallel mechanism," *Mech. Mach. Theory*, vol. 32, no. 8, pp. 895-902, 1997.

[3] J. A. Carretero, R. P. Podhorodeski, M. A. Nahon, C. M. Gosselin, "Kinematic analysis and optimization of a new three degree-of-freedom spatial parallel manipulator," *ASME J. Mech. Design*, vol. 122, no. 1, pp. 17-24, 2000.

[4] J. A. Carretero, M. Nahon, and R. P. Podhorodesk, "Workspace analysis of a 3-dof parallel mechanism," in *Proc. IEEE/RSJ Intl. Conf. Intell. Robots Syst.,* 1998, pp. 1021-1026.

[5] J-P.Merlet, "Optimal design for the micro parallel robot MIPS," in *Proc. Intl.. Conf. Robot. Autom*., 2002, pp. 1149-1154.

[6] K.-M. Lee and D. K. Shah, "Kinematic analysis of a 3-DOF in-parallel actuated manipulator," *IEEE J. Robot., Autom.*, vol. 4, no. 3, pp. 354-360, 1988.

[7] G. B. Chung, B.-J. Yi, I. H. Suh, W. K. Kim, and W. K. Chung, "Design and analysis of a spatial 3-DOF micromanipulator for tele-operation," in *Proc. IEEE/RSJ Intl. Conf. Intell. Robots Syst*., 2001, pp. 337-342.

[8] J. H. Chung, B.-J. Yi, and S. Oh, "Design of a new spatial 3-DOF parallel mechanism with application to a PDP TV mounting device," in *Proc. IEEE/RSJ Intl. Conf. Intell. Robots Syst.,* 2007, pp. 3999-4006.

[9] I. Zabalza, J. Ros, J. J. Gil, J. M. Pintor, and J. M. Jimenez, "Tri-Scott. A micabo like 6-DOF quasi-decoupled parallel manipulator," in *Proc. Workshop Fundamental Issues and Future Research Directions for Parallel Mechanisms and Manipulators*, 2002.

[10] S. Y. Lee, Y. S. Lee, B. S. Park, S. H. Lee, and C. S. Han, "MFR (Multipurpose Field Robot) for installing construction materials," *Autonomous Robots*, vol. 22, no. 3, pp. 265-280, 2007.

[11] S. N. You, S. Y. Lee, H. S. Choi, C. S. Han, K. Y. Lee, and S. H. Lee, "Development of the curtain wall installation robot : Performance and efficiency tests at a construction site," *Autonomous Robots*, vol. 22, no. 3, pp. 281-291, 2007.